

AD-A102 339

ELECTROCHEMICAL TECHNOLOGY CORP SEATTLE WA  
CORROSION OF MAGNESIUM AT HIGH ANODIC POTENTIALS. (U)

F/6 7/4

JUL 81 T R BECK, S G CHAN

N00014-76-C-0495

NL

UNCLASSIFIED

1 rev 1  
AG-5  
02-459

END  
DATE  
FILED  
8-81  
OTIC

ADA1023339

Contract N00014-76-C-0495

12

LEVEL II

CORROSION OF MAGNESIUM AT HIGH ANODIC POTENTIALS

Manuscript

THEODORE R. BECK  
ELECTROCHEMICAL TECHNOLOGY CORP.  
3935 LEARY WAY N.W.  
SEATTLE, WA 98107  
(206) 632-5965

DTIC  
ELECTE  
S D  
AUG 03 1981  
E

INTERIM REPORT FOR PERIOD APRIL 1980 - JUNE 1981

Reproduction in whole or in part is permitted for  
any purpose of the United States Government.  
Distribution is unlimited.

Prepared for

OFFICE OF NAVAL RESEARCH  
800 North Quincy Street  
Arlington, VA 22217

July 1981

DTIC FILE COPY

81 8 03 120

REPORT DOCUMENTATION PAGE		READ INSTRUCTIONS BEFORE COMPLETING FORM
1. REPORT NUMBER	2. GOVT ACCESSION NO.	3. EDITION'S CATALOG NUMBER
4. TITLE (and Subtitle) Corrosion of Magnesium at High Anodic Potentials.		5. PERIODIC REPORTS PERIOD COVERED Technical Report, April 1980 - June 1981
6. AUTHOR(S) Theodore R. Beck and S. G. Chan	7. CONTRACT OR GRANT NUMBER(S) N00014-76-C-0495	8. PROGRAM ELEMENT PROJECT, TASK & WORK UNIT NUMBERS 1621
9. PERFORMING ORGANIZATION NAME AND ADDRESS Electrochemical Technology Corp. 3935 Leary Way N.W. Seattle, WA 98107	10. 11. CONTROLLING OFFICE NAME AND ADDRESS Office of Naval Research Materials Science Division Arlington, VA 22217	
12. REPORT DATE July 1981	13. NUMBER OF PAGES 13	14. MONITORING AGENCY NAME & ADDRESS (if different from Controlling Office)
15. SECURITY CLASS. (of this report) Unclassified	16. DISTRIBUTION STATEMENT (of this Report)	17. DISTRIBUTION STATEMENT (of the abstract entered in Block 20, if different from Report) Reproduction in whole or part is permitted for any purpose of the United States Government. Distribution is unlimited.
18. SUPPLEMENTARY NOTES Manuscript has been submitted to Symposium volume for H. H. Uhlig 75th Birthday Symposium, The Electrochemical Society, Fall Meeting, Denver, October, 1981.	19. KEY WORDS (Continue on reverse side if necessary and identify by block number) Magnesium, corrosion, pitting, mass transport, salt film.	
20. ABSTRACT (Continue on reverse side if necessary and identify by block number) During the pitting of magnesium and other metals in halide solutions, a film of halide salt of the metal forms on the corroding surface. This salt film plays a major role as a diffusion barrier for water and prevents repassivation by oxide. Properties of magnesium chloride layers were determined on corroding high-purity magnesium shielded electrodes or one-dimensional pits. Electrical transient experiments showed that the salt film thickness is proportional to applied anodic potential and that conduction is by the high field mechanism. Water diffusion rate decreases with film thickness.		

Accession For	
NTIS GRA&I	
DTIC TAB	
Unannounced	
Justification	
By _____	
Distribution/	
Availability Codes	
Dist	Avail and/or Special
A	

## CORROSION OF MAGNESIUM AT HIGH ANODIC POTENTIALS

T. R. Beck and S. G. Chan  
Electrochemical Technology Corp.  
3935 Leary Way N.W.  
Seattle, WA 98107

### ABSTRACT

During the pitting of magnesium and other metals in halide solutions a film of halide salt of the metal forms on the corroding surface. This salt film plays a major role as a diffusion barrier for water and prevents repassivation by oxide. Properties of magnesium chloride layers were determined on corroding high-purity magnesium shielded electrodes or one-dimensional pits. Electrical transient experiments showed that the salt film thickness is proportional to applied anodic potential and that conduction is by the high field mechanism. Water diffusion rate decreases with film thickness.

Corrosion of magnesium has been studied in relation to use as structural material in the atmospheric environment (1) as a cathodic protection anode (2) and as an anode in primary cells (3). Other studies have been made of associated thermodynamics (4) and kinetics and transport processes (5-9). Magnesium corrosion is highly hindered by surface hydroxide (8) and the mixed potential for dissolution is generally about one volt positive to the reversible potential of magnesium. The corroded surface is rough and the corrosion product film sometimes contains finely divided reactive magnesium particles (10). Hydrogen is simultaneously evolved so that the apparent valence of dissolution is about 1.4 rather than the standard valence of 2.

The purpose of the present paper is to describe and analyze corrosion of magnesium at high anodic potentials in magnesium chloride solutions in which a magnesium chloride film forms on the corroding surface. Mass transport effects and properties of the salt film are described. The results provide some illumination of corrosion mechanisms at lower anodic potentials.

### Experimental

The experiments described in this paper were carried out with shielded (one dimensional pit) electrodes, described previously (11). The working electrodes were 99.9% pure magnesium rods with 0.16 cm x 32 cm cross section cast in 0.6 cm diameter epoxy resin insulating sheaths. Experiments were conducted in the anode facing up position for hydrodynamic stability, and the corroding surface was observed through a 60 x binocular microscope above the cell. A flow cell that could be put under the microscope (12) was also used. The shielded pit electrodes faced up on the bottom of a 0.32 cm x 0.32 cm cross section flow channel. All of the experiments were carried out in solutions of various concentrations of ACS-specification reagent grade  $MgCl_2 \cdot 6 H_2O$  in distilled water.

Many different types of experiments were conducted with the shielded electrodes to characterize the transport mechanisms. Potentiodynamic polarization curves were measured under stagnant and forced convection conditions. The rate of evolution of hydrogen gas, produced simultaneously with corrosion, was measured in an inverted electrolyte-filled micro gas burette held over the pit. The effect of electrolyte velocity on the limiting current density was determined with a flow system (13) using a Teflon pump and a rotameter calibrated for each solution. Current density transients were measured under potentiostatic conditions in the early stages of development of the diffusion layer in various bulk  $MgCl_2$  concentrations. Potential drop in the pit electrolyte was measured as a function of position with a vertically-calibrated movable Luggin capillary (11).

Electrical transient methods were used to characterize the properties of the salt film on the metal surface. Step potentials were applied in the positive and negative direction to the magnesium anode corroding at steady state conditions. Measured initial peak currents gave electrical conduction properties of the salt film. Integrated current density versus time for a positive step potential gave charge density of incremental amount of salt film formed.

A Wenking Model 68T53 potentiostat and a PAR Model 173 potentiostat were used for the controlled potential experiments. For applied potentials greater than 10 V, a well-filtered variable voltage DC power supply was connected to the working and counter electrodes; the working electrode potential was measured against a saturated calomel reference electrode. Fast electrical transients were measured on a Tektronix Model 564B storage oscilloscope and slow transients on a Hewlett-Packard Model 7046A x-y plotter. A saturated calomel reference electrode was used in stagnant electrolyte experiments and a silver/-silver chloride electrode in contact with the solution in the flow experiments (13).

### Results and Discussion

**Polarization Curves**--A typical potentiodynamic polarization curve for magnesium in  $MgCl_2$  solution is shown in Fig. 1. This curve was obtained in 0.94 M  $MgCl_2$  solution with a sweep rate of 1 V/m in the positive and negative directions. The current density in the approximately linear positive-sweep region from -1.3 V to 2 V is limited by ohmic resistance of the solution. In this region hydrogen bubbles evolve vigorously and cause increasingly unstable current with increase in potential. The corroding metal surface has a jet black appearance due to a microporous surface as observed for titanium in the ohmically-limited region (11, 13).

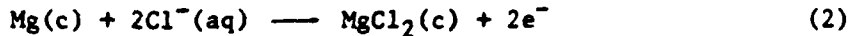
At a potential above 2 V the current density deviates from the linear relationship and decays rapidly due to salt film passivation. The hydrogen evolution rate decreases significantly and the corroding surface becomes electropolished. In the salt film passivation region, agitation of the electrolyte in the pit causes the current density to increase. On the negative sweep from 10 V the current density remains small until the potential is below 0 V. Then the hydrogen evolution increases significantly and the current density rises to the ohmic limit. The zero-current intercept is more negative on the negative sweep because the surface is completely active. On the initial positive sweep starting at -2 V the corrosion initiates at discrete small pits and time is required for the whole surface to become active.

The potential for salt film passivation,  $\phi_p$ , and the corresponding current density,  $i_p$ , both decrease approximately linearly with increasing concentration. At saturation of  $MgCl_2$ , the salt passivation potential is about -1 V and the passivation current density about  $0.2 \text{ A/cm}^2$ . Current density in the ohmic region can be described by (11)

$$i = \frac{K \Delta \phi}{d + a \sqrt{rw}} \quad (1)$$

although the hydrogen bubbles cause some error.

The electrode reaction in the mass transport limited region is



in which a layer of salt covers the metal. The salt layer is assumed to conduct by transport of chloride and/or magnesium ions. Magnesium chloride dissolves at the salt-solution interface and magnesium ions are transported away through the solution.

The standard reversible potential for reaction 2 is calculated from free energy data (14) to be -1.95 V<sub>SCE</sub>. It is not possible to

check this value on a polarization curve such as Fig. 1 because the salt film dissolves as the reversible potential is approached. An ac technique was therefore used.

A sine wave was superimposed through the potentiostat on a pit at +3 V dc in 2.35 M  $MgCl_2$  solution. The current-voltage curve was displayed on the oscilloscope. At frequencies of 10 to 15 Hz the zero-current intercept occurred at  $-1.9 \pm 0.1$  V. At lower frequencies the salt film dissolved and at higher frequencies capacitive charging and discharging of the salt film gave a hysteresis loop. There was a large hysteresis in the anodic current region at 10 to 50 Hz but essentially no hysteresis in the cathodic current region and in the region of the zero-current intercept. The metal surface remained bright under the salt layer in these tests. The zero-current (-1.9 V) intercept appears to be the reversible potential for reaction 2 and will be assumed so in this paper.

The valence of dissolution was determined in the mass transport limited region in 2.35 M  $MgCl_2$  solution at a potential of 5.0 V. At this condition, the corroding metal surface is shiny and the hydrogen evolution rate is small. Four runs were made at 16 hours each starting from a condition of the magnesium polished flush with the epoxy resin surface. The average depth at the end of the runs was measured with a machinist's dial gage and compared to the integrated current from the strip chart recorder. The measured valence was  $2.03 \pm 0.03$ .

*Hydrogen Evolution.*--The rate of hydrogen evolution was measured in 0.94 M  $MgCl_2$  solution at potentials from -1.5 V to 19 V. The volumetric rate ( $cm^3/s$ ) was converted to an equivalent cathodic hydrogen current density using the ideal gas law and Faraday's law.

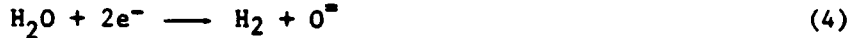
$$i_{H_2} = \frac{2F v (273)(76 - p)}{22,400 T(76)A} \quad (3)$$

The ratio of the hydrogen current density to the actual anodic current density is plotted versus potential in Fig. 2. The actual anodic current density is assumed to be the sum of the absolute values of the measured anodic current density and the hydrogen current density.

The ratio,  $i_{H_2}/i_a$ , is approximately constant at 0.3 for the ohmic limited region; both  $i_{H_2}$  and  $i_a$  increased with potential. This value corresponds to an apparent valence of 1.4, which is in general agreement with literature values (10). The ratio,  $i_{H_2}/i_a$ , is about two orders of magnitude smaller at high potentials in the mass transport limited region. In each of these experiments between 0.5 V and 19 V in the mass transport limited region the hydrogen was collected over a period of time in which the average measured current was in the range,  $0.15 \pm 0.07$  A/cm<sup>2</sup>. The ratio,  $i_{H_2}/i_a$ , decreases with increase in

potential in this region.

An hypothesis is made here that the rate of hydrogen generation in the mass transport limited region is directly related to the rate of water diffusion through the salt layer. Because the metal/salt interface is at a very negative potential (-1.9 V) it will be assumed that every water molecule arriving at the interface is reduced to hydrogen



The small concentration of oxide ions simultaneously formed will be incorporated into the salt film as magnesium oxychloride.

The current density for hydrogen generation is therefore

$$i_{\text{H}_2} = \frac{2F D_W \Delta C_W}{t} \quad (5)$$

It will be assumed there that the salt film thickness is directly proportional to the potential across the salt film

$$t = K_1 (\phi + 1.9) \quad (6)$$

(The value of  $K_1$  is discussed in a later section.) Equations 5 and 6 may be combined to give the linear relation

$$1/i_{\text{H}_2} = K_2 (\phi + 1.9) \quad (7)$$

Experimental values of  $1/i_{\text{H}_2}$  in the mass transport limited region are plotted versus  $\phi$  in Fig. 3. The least-squares line has a slope of 272  $(\text{A}/\text{cm}^2)\text{-}1 \text{ V}^{-1}$  and an intercept of -4 V. The dashed line in Fig. 3 was drawn through a zero-current intercept of -1.9 V in accordance with Eq. 7, and gives a line

$$1/i_{\text{H}_2} = 325 (\phi + 1.9) \quad (8)$$

The data thus appear to be in reasonable accord with the hypothesis of water transport in the salt film. The dashed curve in Fig. 2 is

$$\frac{i_{\text{H}_2}}{i_a} = \frac{1}{(0.15)(325)(\phi + 1.9)} = \frac{0.0205}{(\phi + 1.9)} \quad (9)$$

*Effect of Electrolyte Velocity*--The effect of electrolyte velocity on current density in the mass transport limited region is shown in Fig. 4. These experiments were conducted in 2.35 M  $\text{MgCl}_2$ . The depth

of the recessed Mg electrode in the side of the flow channel was about 0.15 cm. The strong relation of current density to flow velocity shows that the current is mass transport limited, although the slope with potential at the higher flow rates indicates partial kinetic control.

*Conductivity of Solution in Pit--Potential in the pit solution was measured as a function of depth with the position-calibrated small Luggin capillary (11) for bulk concentrations of 0.94, 2.35 and 4.7 M. Pit depths were 0.2 to 0.3 cm. Solution conductivity calculated from the slope of the potential versus depth curves varied smoothly from the saturation value at the bottom of the pit to the bulk concentration near the mouth. The pits with magnesium did not have the extremely-viscous, low-conductivity solutions near the bottom that were observed in pits with titanium (11).*

*Current Density-Time Transients--Experiments were conducted in which a step potential from the open-circuit value to +5.0 V was applied for a range of bulk  $MgCl_2$  concentrations. The pit depth averaged  $0.09 \pm 0.01$  cm in these experiments. Current density-time transients are shown in Fig. 5. The initial current is ohmically limited. Salt passivation initiates in the time period, 0.01 to 0.1 s. By 1 s the salt film is fully developed and thereafter the current density decays as the diffusion layer thickness increases in the pit. At about 1000 s the current density levels to the steady-state value for a diffusion layer thickness corresponding to the pit depth. The decrease in current density with bulk concentration of  $MgCl_2$  in the unsteady-state and steady state regions clearly indicate a mass transport limit for  $Mg^{++}$  ion.*

In the unsteady-state region the limiting current density can be described (15) by

$$i_L = \frac{zF(C_s - C_b)}{t_d} \sqrt{\frac{D}{\pi}} \quad (10)$$

and in the steady-state region it can be described by

$$i_L = \frac{zFD(C_s - C_b)}{t_d} \quad (11)$$

The chloride ion transference number has a value of about 0.79 (16) in concentrated  $MgCl_2$  solution concentrations shown in Fig. 5. Values of D were calculated from Eq. 10 and 11 and Fig. 5 for bulk concentrations from 0.94 to 4.23 M. The values were  $1.1 \pm 0.1 \times 10^{-5} \text{ cm}^2/\text{s}$  for the unsteady state curves and  $1.8 \pm 0.2 \times 10^{-5} \text{ cm}^2/\text{s}$  for the steady state curves, assuming  $d = 0.1$  cm. These values are many times larger than

would be expected in concentrated solution. A possible cause of the large apparent diffusivities is convective mixing by the hydrogen bubbles of the high concentration solution from the pit bottom to the lower concentration at the pit mouth. Quantitative measurements and calculations remain to be made.

A surprising result in Fig. 5 is that the current density did not go to zero in saturated solution but also followed the same  $-1/2$  power law of Eq. 10. The experiments were repeated a number of times with solution that was saturated with  $MgCl_2$  at  $30^\circ$  or  $50^\circ C$  before pouring into the cell to insure saturation in the cell which was run at  $21^\circ C$ . Curve a is for initial  $30^\circ C$  saturated solution and curve b is for initial  $50^\circ C$  saturated solution. The pit was filled with solution-precipitated  $MgCl_2 \cdot 6 H_2O$  crystals for the  $50^\circ C$  solution but not the  $30^\circ C$  solution. The solution next to the salt film appears to be supersaturated so that the transport can be described by

$$i_L = \frac{zF (C^* - C_s)}{t} \sqrt{\frac{D}{\pi r}} \quad (12)$$

The degree of supersaturation calculated from Eq. 12 and curve a Fig. 5 for  $D = 1.1 \times 10^{-5} \text{ cm}^2/\text{s}$  is  $1.5 \pm 0.3\%$  above saturation. Supersaturation for curve b is calculated to be about 3% above saturation.

*Step Potential Polarization Curves*--Step potential experiments were conducted with Mg in 4.23 M (90% saturated)  $MgCl_2$  solutions in order to determine electrical properties of the  $MgCl_2$  salt film over a wide range of potential. Potential was stepped up and down from an initial  $\phi_1$  to a value of  $\phi_2$  starting with same initial current density of  $0.02 \text{ A/cm}^2$ . The potential range of  $\phi_1$  was from 1 V to 10 V. The initial peak current density,  $i_p$ , at each value of  $\phi_2$  was recorded on the storage oscilloscope. The data are plotted semilogarithmically in Fig. 6.

A linear relationship is obtained at current densities below  $0.02 \text{ A/cm}^2$  in accordance with high-field conduction.

$$i = i_0 \exp \left( \frac{\beta \phi_2}{t_1} \right) \quad (13)$$

At higher current densities the data deviate from the linear relationship due to an apparent series ohmic resistance. The value of  $\beta/t_1$  or  $t_1/\beta$  can be calculated from the linear region from the derivative of Eq. 13.

$$t_1/\beta = \left( \frac{1}{2.30} \right) \left( \frac{d\phi}{d \log i} \right) \quad (14)$$

Values of  $d\psi/d\log i$  determined from Fig. 6 are plotted versus potential,  $\phi_1$ , in Fig. 7. The data appear to be linear with potential, consistent with the salt film thickness being linear with potential and a constant  $\beta$ . The dashed line in Fig. 7 is drawn through the reversible potential

$$t_1/\beta = 0.098 (\phi_1 + 1.9) \quad (15)$$

The value of  $i_o$  in Eq. 13 is about  $1 \times 10^{-6} \text{ A/cm}^2$  from Fig. 6.

The difference between a curve at high current density and the extrapolated linear region in Fig. 6 gives an apparent ohmic potential difference. Plots of these potential differences versus current density are approximately linear and give generally increasing resistances from 270 to 770 ohms (14 to  $29 \Omega \text{ cm}^2$ ) for potentials from 1 to 10 V. The solution resistance for an effective 0.2 cm deep pit is about 40 ohms based on conductivity data. It appears that there is a series ohmic resistance in the pit, perhaps a porous salt layer on top of the barrier salt layer.

Attempts were made to determine the incremental amount of barrier layer film growth for a step potential. In general, the current density increases at the step potential to a value above the mass transport limited current density,  $i_L$ , and decays in time back to  $i_L$ . It was assumed that the area under this curve would represent the charge for incremental amount of barrier layer film. In practice there were complications that caused the method to give only a rough approximation; the poststep value of  $i_L$  was not always identical to the prestep value, and there was a double overshoot in current density due to concentration changes in the solution side. Nevertheless the average incremental thickness appeared to be about  $50 \text{ \AA/V}$  at a limiting current density of  $1 \text{ mA/cm}^2$ . The value of  $\beta$  can be estimated from this value of  $dt_1/d\phi_1$  in the derivative of Eq. 15.

$$\beta = 10 \frac{dt_1}{d\phi_1} \approx 5 \times 10^{-6} \text{ cm/V} \quad (16)$$

This value is similar to values obtained for oxide films (17). The value of  $dt/d\phi$  decreased with increasing current density. The data were too scattered to determine if there was a trend in  $dt/d\phi$  with potential.

*Permeability of Water and Hydrogen in Salt Film*--The permeability of the  $\text{MgCl}_2$  salt film barrier layer to water and hydrogen is examined here. Solubilities of water and hydrogen in  $\text{MgCl}_2$  are not known, so the permeability,  $P = DC$ , will be calculated. A common unit for permeability is  $\text{cm}^3(\text{STP}) \text{ s}^{-1} \text{ cm}^{-2} \text{ cm} (\text{cm Hg})^{-1}$ . The current density for water reduction based on reaction 4 is then

$$i_w = \frac{2F P_w \Delta p_w}{22,400 t} \quad (17)$$

The value of  $t$  can be expressed by

$$t = 50 \times 10^{-8} (\phi + 1.9) \quad (18)$$

Equation 8 can be rewritten

$$i_{H_2} = \frac{1}{325(t + 1.9)} \quad (19)$$

Assuming  $i_w = i_{H_2}$ , Eq. 17, 18, and 19 may be combined and solved for  $P_w$

$$P_w = \frac{(50 \times 10^{-8})(22,400)}{(325)(2)F \Delta p_w} \quad (20)$$

at 25°C a saturated  $MgCl_2$  solution has a water vapor pressure of 0.789 cm (18). This value in Eq. 20 gives  $P_w = 2.3 \times 10^{-10} \text{ cm}^3(\text{STP}) \text{ s}^{-1} \text{cm}^{-2} \text{ cm} (\text{cm Hg})^{-1}$ .

A question arises whether this value of  $P_w$  is reasonable. A search was made for water permeability of inorganic salts at room temperature. Data were found for a few alkali halides only (18, 19), determined by destruction by water vapor of color centers in crystals. A value calculated from data for KI at 25°C (18) is  $0.004 \times 10^{-10} \text{ cm}^3(\text{STP}) \text{ s}^{-1} \text{cm}^{-2} \text{ cm} (\text{cm Hg})^{-1}$ . Another 25°C value for KI extrapolated from 200° - 300°C data (19) is  $0.0004 \times 10^{-10} \text{ cm}^3(\text{STP}) \text{ s}^{-1} \text{cm}^{-2} \text{ cm} (\text{cm Hg})^{-1}$ . Extrapolated values for KBr and KCl are smaller. Permeabilities of water through various plastics range from  $0.25 \times 10^{-10}$  to  $12,000 \times 10^{-10} \text{ cm}^3(\text{STP}) \text{ s}^{-1} \text{cm}^{-2} \text{ cm} (\text{cm Hg})^{-1}$  with a mean of about  $1000 \times 10^{-10}$  (20). The value of  $P_w$  calculated from  $MgCl_2$  therefore appears to have a reasonable order of magnitude but it remains to be determined by independent measurements if the value is correct.

Another question concerns the feasibility of hydrogen transport out through the  $MgCl_2$  film. Diffusion coefficients for  $H_2$  through KI, KBr, and KCl at 200° - 300°C have been measured (21) but no solubility data were found to convert to permeability. On the other hand, permeability data of  $H_2$  through plastics (20) are available and average about 1/100 the water value, or  $\sim 10 \times 10^{-10} \text{ cm}^3(\text{STP}) \text{ s}^{-1} \text{cm}^{-2} \text{ cm} (\text{cm Hg})^{-1}$ . If it is assumed for example that the permeability of  $H_2$  is 1/100 the value for water, an estimate of the  $H_2$  transport rate can be made from

$$i_{H_2} = \frac{2 F P_{H_2} \Delta p_{H_2}}{22,400 t} \quad (21)$$

The ratio of  $H_2$  to water flux is therefore

$$\frac{i_{H_2}}{i_w} = \frac{P_{H_2} \Delta p_{H_2}}{P_w \Delta p_w} = 0.01 \frac{\Delta p_{H_2}}{\Delta p_w} \quad (22)$$

The value for  $\Delta p_{H_2}$  is 76 S cm Hg in which S is the supersaturation ratio, which may be very large for nucleation of  $H_2$  bubbles in the salt film. The value of  $\Delta p_w$  above is  $\sim 0.8$  cm Hg so that  $i_{H_2}/i_w \approx 0.95$  S. The  $H_2$  permeability rate therefore appears to be adequate based on the above assumptions.

### Conclusions

Corrosion experiments with a shielded high-purity magnesium anode in various concentrations of magnesium chloride showed the following. At high anodic potentials, magnesium ion transport in solution becomes limiting and a barrier layer salt film forms on the metal surface. Electrical conduction of the salt film is by the high-field mechanism and the constants were determined. Thickness is proportional to applied potential. Water diffuses through the salt film leading to hydrogen evolution, with a rate inversely proportional to potential and film thickness.

### Acknowledgment

This work was carried out under Office of Naval Research Contract No. N00014-76-C-0495.

### REFERENCES

1. G. D. Bengough and L. Whitby, *Trans. Inst. Chem. Eng.*, 11, 176 (1933).
2. H. A. Robinson, *Trans. Electrochem. Soc.*, 96, 485 (1946).
3. R. Glicksman and C. L. Morehouse, *J. Electrochem. Soc.*, 102, 273 (1955).
4. G. E. Coates, *J. Chem. Soc.*, 478 (1945).
5. G. E. Coates, *J. Chem. Soc.*, 484 (1945).
6. C. V. King and W. H. Cathcart, *J. Am. Chem. Soc.*, 59, 63 (1937).
7. G. R. Hoey and M. Cohen, *J. Electrochem. Soc.*, 105, 249 (1948).
8. J. L. Robinson and P. F. King, *J. Electrochem. Soc.*, 108, 36 (1961).
9. P. F. King, *J. Electrochem. Soc.*, 110, 1113 (1963).
10. W. J. James, p 128-33, in *Advances in Corrosion Science and Technology*, Vol. 4, Fontana and Staehle, Eds., Plenum Press, New York, 1974.
11. T. R. Beck, *J. Electrochem. Soc.*, 120, 1317 (1973).

12. T. R. Beck, Submitted to J. Electrochem Soc.
13. T. R. Beck, Corrosion, 33, 9 (1977).
14. W. M. Latimer, Oxidation Potentials, 2nd Ed., Prentice Hall, Englewood Cliffs, N.J., 1952.
15. G. Kortum, Treatise on Electrochemistry, 2nd Ed., Elsevier, New York, 1965.
16. T. W. Chapman and J. Newman, A Compilation of Selected Thermodynamic and Transport Properties of Binary Electrolytes in Aqueous Solution, Lawrence Radiation Laboratory Report, UC-4 Chemistry, TID-4500, May, 1968.
17. L. Young, Anodic Oxide Films, Academic Press, New York, 1961.
18. T. J. Neubert and D. L. Roskelley, J. Phys. Chem. Solids, 34, 493 (1973).
19. C. Ruhenbeck, Z. Phys., 207, 446 (1967).
20. J. Brandrup and E. H. Immergut, Eds., Polymer Handbook, III-229, John Wiley, New York, 1975.
21. H. Grundig and C. Ruhenbeck, Z. Phys., 249, 269 (1972).

#### Nomenclature

$a$  = constant  
 $A$  = area,  $\text{cm}^2$   
 $C$  = concentration,  $\text{mol}/\text{cm}^3$   
 $d$  = depth, cm  
 $D$  = diffusivity,  $\text{cm}^2/\text{s}$   
 $F$  = Faraday, 96,500 C/equiv  
 $i$  = current density,  $\text{A}/\text{cm}^2$   
 $i_0$  = exchange current density,  $\text{A}/\text{cm}^2$   
 $K$  = constant  
 $l$  = length, cm  
 $p$  = pressure, cm Hg  
 $P$  = permeability,  $\text{cm}^3(\text{STP}) \text{ s}^{-1} \text{ cm}^{-2} \text{ cm} (\text{cm Hg})^{-1}$   
 $t$  = thickness, cm  
 $t_+$  = transference number  
 $T$  = absolute temperature  
 $v$  = volumetric rate of  $\text{H}_2$  evolution,  $\text{cm}^3/\text{s}$   
 $w$  = width, cm  
 $z$  = valence, equiv/mol  
 $\bar{z}$  = exponential constant,  $\text{cm}/\text{V}$   
 $\tau$  = time, s  
 $\dot{\tau}$  = potential, V

#### Subscripts

$a$  = anodic  
 $b$  = bulk  
 $e$  = electrolyte  
 $\text{H}_2$  = hydrogen  
 $L$  = limiting  
 $p$  = peak  
 $s$  = saturation  
 $w$  = water

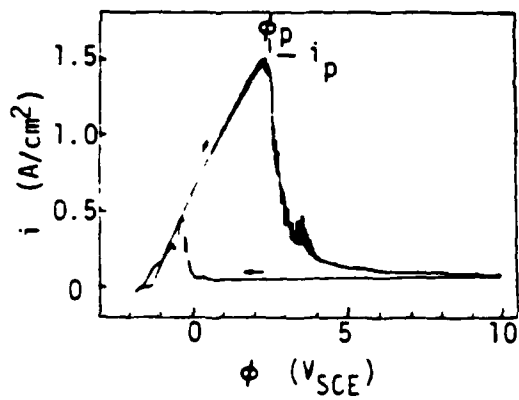


Fig. 1. Potentiodynamic polarization curve for magnesium in 0.94 M  $\text{MgCl}_2$ ; depth = 2 mm; sweep rate = 1 V/min.

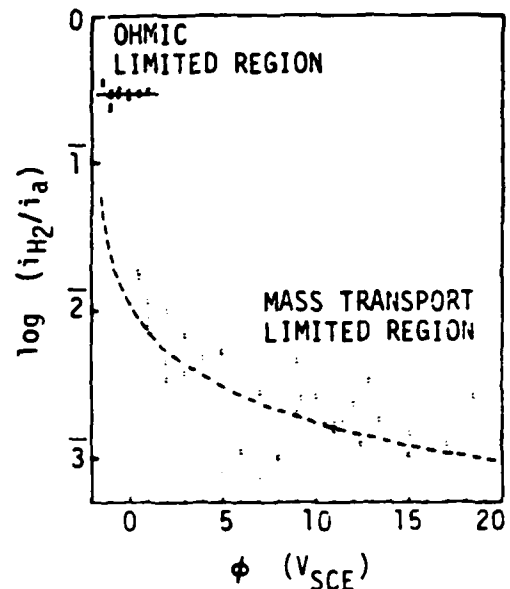


Fig. 2. Ratio of hydrogen current density to anodic current density in ohmic limited and mass transport limited regions for 0.94 M  $\text{MgCl}_2$ .

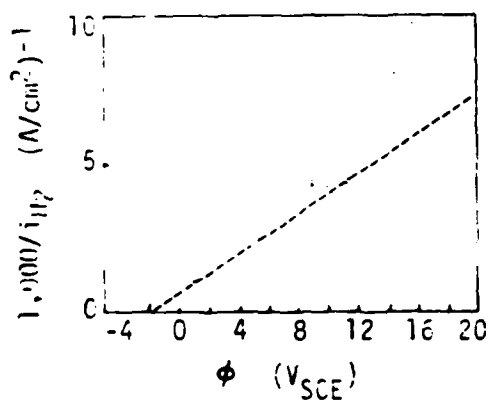


Fig. 3. Plot of reciprocal of hydrogen evolution current density versus potential (Eq. 7) for mass transport limited region with 0.94 M  $\text{MgCl}_2$ .

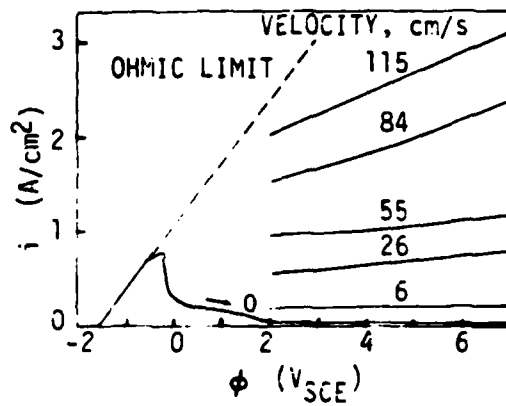


Fig. 4. Effect of electrolyte velocity on current density in mass transport limited region in 4.7 M  $\text{MgCl}_2$ ; depth = 1.5 mm.

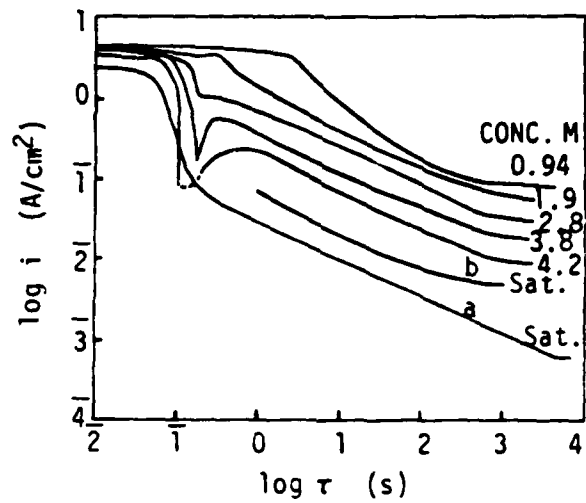


Fig. 5. Current-time transients for Mg in  $MgCl_2$  solutions at  $\phi = 5.0$  VSCE; depth = 0.9 mm; a = cooled from  $30^\circ C$ , b = cooled from  $50^\circ C$  to  $21^\circ C$ .

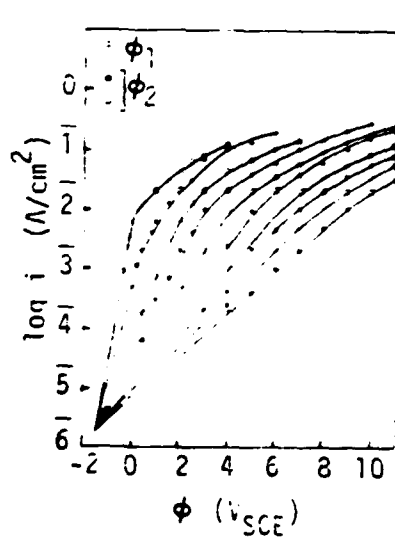


Fig. 6. Plots of initial current densities after step potential to  $\phi_2$  from  $\phi_1$  in 4.2 M  $MgCl_2$ .

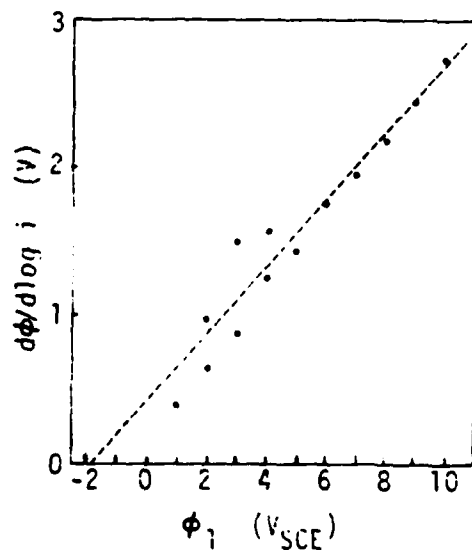


Fig. 7. Plot of slopes from Fig. 6 versus  $t_1$ .